ACS APPLIED MATERIALS & INTERFACES

Letter

www.acsami.org

Integration of Self-Assembled Vertically Aligned Nanocomposite $(La_{0.7}Sr_{0.3}MnO_3)_{1-x}$:$(ZnO)_x$ Thin Films on Silicon Substrates

Wenrui Zhang,[†] Aiping Chen,[‡] Fauzia Khatkhatay,[‡] Chen-Fong Tsai,[†] Qing Su,[†] Liang Jiao,[†] Xinghang Zhang,[†,§] and Haiyan Wang*[,†,‡]

[†]Materials Science and Engineering Program, [‡]Department of Electrical and Computer Engineering, and [§]Department of Mechanical Engineering, Texas A&M University, College Station, Texas 77843, United States

ABSTRACT: Epitaxial $(La_{0.7}Sr_{0.3}MnO_3)_{1-x}$:$(ZnO)_x$ (LSMO:ZnO) in vertically aligned nanocomposite (VAN) form was integrated on STO/TiN-buffered silicon substrates by pulsed-laser deposition. Their magnetotransport properties have been investigated and are systematically tuned through controlling the ZnO concentration. The composite film with 70% ZnO molar ratio exhibits a maximum magnetoresistance (MR) value of 55% at 70 K and 1 T. The enhanced tunable low-field MR properties are attributed to structural and magnetic disorders and spin-polarized tunneling through the secondary ZnO phase. The integration of LSMO:ZnO VAN films on silicon substrates is a critical step enabling the application of VAN films in future spintronic devices.

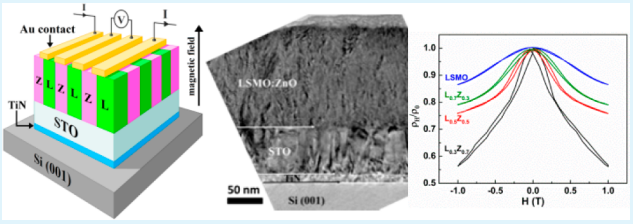

KEYWORDS: *vertically aligned nanocomposites (VAN), epitaxy, thin films, low-field magnetoresistance (LFMR), pulsed-laser deposition, spintronics*

INTRODUCTION

Strongly correlated complex oxides have generated a wide spectrum of intriguing phenomena because of the interactions of charge, spin, orbital, and lattice degrees of freedom across their heterointerfaces, including unusual electronic reconstruction at adjoined heterointerfaces,[1] colossal magnetoresistance (MR),[2] and, more recently, multiferroic interface coupling.[3] This has led to extensive research on exploration of the fundamental physics, epitaxial design of heterointerfaces based on atomic terminations, and the ultimately diversified functionalities for potential devices.[4] However, most previous studies focused on heteroepitaxial layer-by-layer assembly because of its fine control of film compositions and configurations,[5,6] and research on vertically aligned structures and their vertical interfacial coupling effects is new and scarce. An early vertical two-phase oxide system was demonstrated in $(La_{0.67}Ca_{0.33}MnO_3)_{1-x}$:$(MgO)_x$ (LCMO:MgO) thin films in an effort to investigate the structural transition of the LCMO phase.[7] Afterward, the morphology dependence of $BiFeO_3$:$CoFe_2O_4$ nanostructures on substrate orientations was reported, which provided an effective platform for the further study of magnetoelectric coupling.[8]

Self-assembled vertically aligned nanocomposite (VAN) thin films were first introduced in $BiFeO_3$:Sm_2O_3 and $La_{0.7}Sr_{0.3}MnO_3$ (LSMO):ZnO systems through careful material selection and microstructure control.[9] Unique and new functionalities also arise from such ordered structures, such as a reduced clamping effect from substrates and more efficient interfacial coupling.[10,11] For example, a very large vertical tensile strain was maintained in the $BiFeO_3$:Fe_3O_4 VAN films, resulting in enhanced saturation magnetization compared to its bulk value.[12] Meanwhile, tunable vertical lattice strain and dielectric property control in $BiFeO_3$:Sm_2O_3,[13] low-field MR (LFMR) in LSMO:ZnO[14,15] and $(LSMO)_{0.5}$,[16] and multifunctionality in $PbTiO_3$:$CoFe_2O_4$ films have also been demonstrated in VAN systems.[17] Although research on functional oxides has made tremendous progress in the past decades, most of the VAN studies focus on films grown on single-crystal perovskite and perovskite-related oxide substrates, including $SrTiO_3$ (STO), $LaAlO_3$, $DyScO_3$, $NdGaO_3$, etc., to achieve high epitaxial quality.[18] Such single-crystal substrates are expensive and in small dimension, thus not desirable for large-scale integration of oxide thin films with conventional semiconductor devices. Therefore, it is highly attractive to grow these unique VAN thin films on traditional semiconductor substrates such as silicon (Si) while maintaining a satisfactory performance. Unfortunately, the direct growth of functional oxides on Si often fails to achieve highly epitaxial films because of oxidation on Si during high-temperature deposition and large lattice mismatch. One possible solution is to grow a buffer layer to provide structural compatibility, thermal stability, and chemical stability between thin films and underlying substrates.[19] The buffer layers demonstrated include STO,[20] yittra-stabilized zirconia (YSZ)/$YBa_2Cu_3O_{7-\delta}$,[21] $Bi_4Ti_3O_{12}$/CeO_2/YSZ,[22] etc.

In this work, for the first time, we demonstrate the integration of epitaxial VAN films on Si substrates using a bilayer buffer structure. For this demonstration, a LSMO:ZnO

Received: January 7, 2013
Accepted: April 25, 2013
Published: April 25, 2013

   dx.doi.org/10.1021/am400068h | ACS Appl. Mater. Interfaces 2013, 5, 3995−3999

VAN system has been selected for this study based on our prior success in growing $(LSMO)_{0.5}$:$(ZnO)_{0.5}$ VAN films on single-crystal STO substrates with a tunable LFMR property.[14] The TiN/STO bilayer buffer layer has been deposited to avoid surface oxidation and reduce the lattice mismatch between VAN films and underlying substrates. The magnetotransport property of the as-deposited VAN thin films has been investigated, which shows a performance comparable to those grown on STO single-crystal substrates. Therefore, this work demonstrates promises in bridging the gap to integrate VAN films in future spintronic devices.

EXPERIMENTAL SECTION

The composite targets with different composition ratios were prepared by a conventional ceramic sintering method. In brief, the stoichiometric mixture of high-purity La_2O_3, $SrCO_3$, and MnO_2 powders was ground, pressed, and then sintered at 1200 °C for 24 h to synthesize LSMO powders. The calcined LSMO powders were then mixed with ZnO powders in different ratios, pressed into disks, and subsequently sintered at 1300 °C for 12 h to make the composite targets. TiN and STO buffer layers and $L_{1-x}Z_x$ thin films were deposited subsequently on Si (001) substrates by pulsed laser deposition (PLD) at a base pressure of 1.5×10^{-6} Torr. The substrate temperature was set at 750 °C for all deposited films. Also, the TiN and STO buffer layers were grown at vacuum and an oxygen pressure of 40 mTorr, respectively. The composite films were deposited at an optimized oxygen pressure of 200 mTorr. After deposition, the composite thin films were cooled in 200 Torr oxygen at a cooling rate of 10 °C/min.

The composition and microstructure of as-prepared films were investigated by X-ray diffraction (XRD; PANalytical Empyrean), transmission electron microscopy (TEM; FEI Tecnai G2 F20) operated at 200 kV. Cross-sectional samples for TEM observation were prepared by a standard manual grinding and thinning of samples with a final ion-milling step (Gatan PIPS 691 precision ion polishing system). For electrical property measurement, gold electrodes were deposited by sputtering on top of thin films with a shadow mask method. The conventional four-probe resistivity method was used to test the resistivity of as-deposited samples with a commercial physical property measurement system (Quantum Design PPMS 6000). The test temperature was chosen to be in the range of 20−340 K, and the magnetic field was up to 1 T.

RESULTS AND DISCUSSION

Figure 1a shows the typical XRD pattern of a $LSMO_{0.3}$:$ZnO_{0.7}$ ($L_{0.3}Z_{0.7}$) thin film on a Si substrate buffered with a TiN/STO bilayer. For comparison, the XRD pattern of a pure LSMO thin film grown on Si substrates is also shown. It is obvious that the peaks from LSMO and STO in $L_{0.3}Z_{0.7}$ composite films are almost the same as those in a pure LSMO film, indicating that there is no reaction or impurity phase in the composite thin films. Both the LSMO phase and the STO buffer layer have grown preferentially along the [00*l*] orientation, while the ZnO phase has oriented along the $[11\bar{2}0]$ orientation. A small peak from TiO_2 (004) was observed, which is possible from minor oxidation of the TiN layer when depositing STO in an oxygen atmosphere. No peak from the TiN buffer was identified in the complete XRD θ−2θ scan possibly because of the very thin TiN layer. Figure 1b gives the φ scans of the Si (202), LSMO (202), and ZnO $(10\bar{1}0)$ planes. It is interesting to note that LSMO ($d_{LSMO\langle 100\rangle}$ = 3.87 Å) has achieved epitaxial cube-on-cube growth on Si ($d_{Si\langle 100\rangle}$ = 5.43 Å) without any rotation assisted by the bibuffer layer. This is possibly due to the large lattice mismatch of Si-TiN (24.6%) and TiN-STO (7.9%), which led to direct domain-matching growth of STO ($d_{STO\langle 100\rangle}$ = 3.96 Å) and TiN ($d_{TiN\langle 100\rangle}$ = 4.24 Å) on Si substrates. The vacuum-deposited TiN layer also acts as oxygen diffusion barrier and protects underlying substrates from oxidation, which usually causes serious problems for epitaxial growth of oxides on Si substrates. The φ scan of the hexagonal ZnO phase exhibits a 4-fold symmetry, which suggests two possible matching relationships with the buffer layer. Thus, the orientation relationships between the VAN films, buffer layers, and Si substrates are determined to be $(001)_{LSMO}\|(11\bar{2}0)_{ZnO}\|(001)_{STO}\|(001)_{TiN}\|(001)_{Si}$, $[110]_{LSMO}\|[0001]_{ZnO}\|[110]_{STO}\|[110]_{TiN}\|[110]_{Si}$, and $[1\bar{1}0]_{LSMO}\|[0001]_{ZnO}\|[1\bar{1}0]_{STO}\|[1\bar{1}0]_{TiN}\|[1\bar{1}0]_{Si}$.

The low-magnification bright-field TEM image of the $L_{0.3}Z_{0.7}$ VAN film shown in Figure 2a demonstrates that self-assembled growth of LSMO and ZnO columns has been achieved on buffered Si substrates. Also, the thicknesses of TiN, the STO

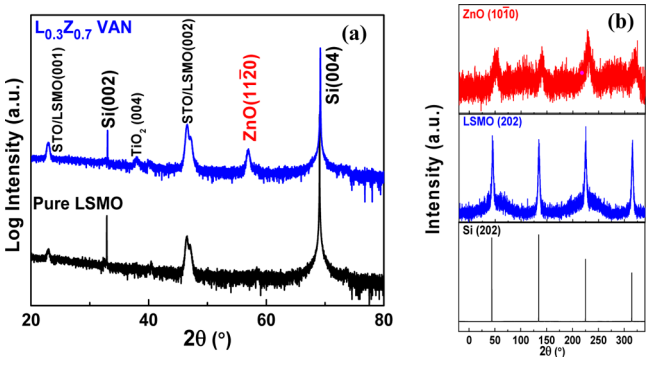

Figure 1. (a) XRD patterns of pure LSMO and $L_{0.3}Z_{0.7}$ composite thin films. (b) φ scans of the Si (202), LSMO (202), and ZnO $(10\bar{1}0)$ planes.

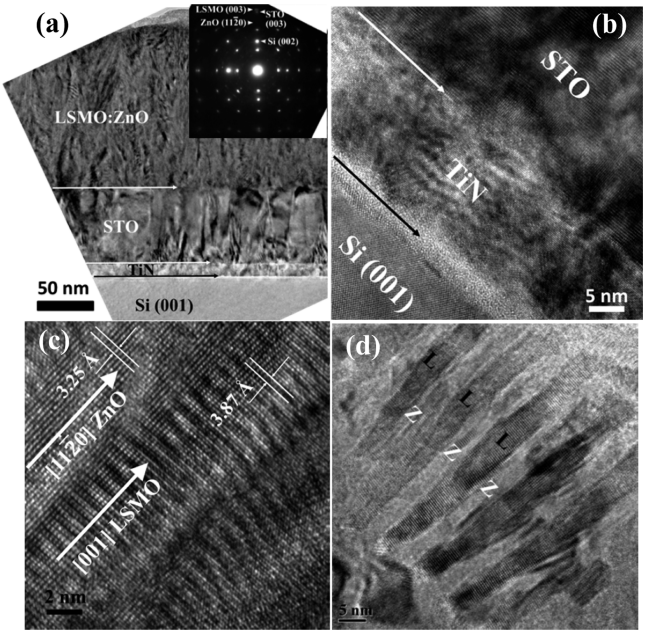

Figure 2. (a) Cross-sectional TEM image of the $L_{0.3}Z_{0.7}$ VAN film. Inset: corresponding SAED image of the $L_{0.3}Z_{0.7}$ VAN film. (b) HRTEM image of interfaces between the Si substrate and buffer layers. (c) Representative high-resolution cross-sectional and (d) plane-view TEM images of the $L_{0.3}Z_{0.7}$ VAN film. LSMO and ZnO are marked as L and Z, respectively, in the above figures.

buffer layer, and the $L_{0.3}Z_{0.7}$ film are determined to be about 15, 100, and 220 nm, respectively. The arrows indicate the abrupt interfaces between each layer. The corresponding selected-area electron diffraction (SAED) pattern is shown as the inset. The distinct diffraction dots from LSMO and ZnO suggest clear phase separation in the VAN films. Figure 2b shows a high-resolution TEM (HRTEM) image of the interfaces between the buffer layer and substrates. A very thin SiO_2 layer of 3−5 nm was observed, which is possible due to minor oxidation of Si substrates as they approached the target deposition temperature. Also, the TiN and STO layers have maintained epitaxial growth on Si substrates, and no diffusion was observed between these layers. The HRTEM image in Figure 2c reveals high-quality epitaxial growth of the LSMO and ZnO nanocolumns on the Si substrates. Both the LSMO and ZnO phases have been marked out based on their lattice parameter, indicating clear phase separation. Figure 2d gives a plane-view TEM image of the $L_{0.3}Z_{0.7}$ composite thin film, which shows ordered alternative growth of the LSMO and ZnO domains. Therefore, all of the above results demonstrate that epitaxial LSMO:ZnO VAN films have been successfully grown on Si substrates.

To investigate the effect of the ZnO phase on the magnetotransport property of the composite thin films, the in-plane resistivity measurement has been conducted for all samples. Figure 3a shows a schematic drawing of the $L_{1-x}Z_x$/STO/TiN/Si field-effect device, which was used to measure the sheet resistance as a function of the magnetic field and temperature. This spintronic device could act as a basic cell to be integrated for magnetic random access memory, which offers significant advantages such as nonvolatile memory, increased data processing speed, and integration density, to a conventional data storage device. The temperature dependence of the normalized zero-field resistivity of $L_{1-x}Z_x$ composite thin films with different ZnO concentrations is compared in Figure 3b. Well-defined metal−insulator transitions (MITs) are observed for samples with a ZnO molar ratio of less than 50%, after which their resistivity becomes too large for measurement and exhibits insulating-like behavior in the entire test temperature range. It is reasonable to consider that ρ is significantly affected by the insulating ZnO phase because the overall resistivity increases as the ZnO concentration increases. Meanwhile, the grain and phase boundaries play important roles as scattering regions for transport properties in the ZnO-rich composite films, thus increasing the resistivity of the VAN films. Figure 3c summarizes the variation of resistivity of the $L_{1-x}Z_x$ VAN films at 160 K in the left y axis as a function of the ZnO compositions. Also, the percolation threshold in conductivity of our VAN films is estimated to be around 70% of ZnO molar ratio, above which the resistance grows drastically. The abrupt change of resistivity on the conduction threshold has also been reported in other LSMO-based composites previously.[23,24] This behavior can be explained by a classical percolation theory. In this theory, the electrical conductivity σ of a "metal−insulator" composite obeys the power law

$$\sigma \propto (x - x_c)^p \quad (1)$$

where x represents the volume fraction of the conduction phase LSMO ("metal" in this system), x_c is the critical percolation value, and p is a critical exponent with a predicted universal value of 1.9 ± 0.2.[25,26] The inset in Figure 3c shows the fitting curve of eq 1 to the experiment data. The fitting relationship shows that the conductivity exponent is very close to the predicted value and the calculated conduction threshold value is

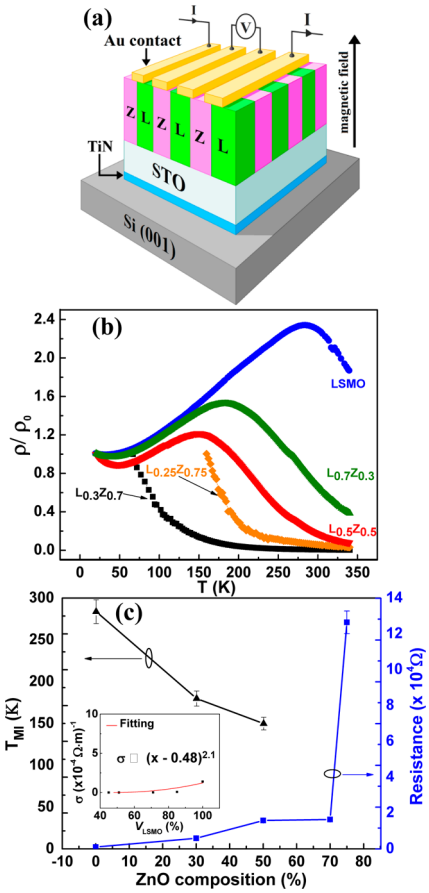

Figure 3. (a) Schematic drawing of the $L_{1-x}Z_x$/STO/TiN/Si field-effect device. (b) Temperature dependence of the normalized zero-field resistivity ρ/ρ_0 of the LSMO:ZnO composite thin films and of pure LSMO films at 0 T. ρ_0 represents resistivity at its lowest measured temperature. (c) T_{MIT} and resistance at 160 K of VAN films shown in the left and right axes, respectively, as a function of the ZnO composition at 0 T. Inset: fitting results of the conductivity of $L_{1-x}Z_x$ VAN films based on the percolation conduction model.

0.48 ± 0.05 of LSMO in volume fraction, which corresponds to 72.5 ± 2.8% of ZnO ("insulator" in this system) molar ratio. The good agreement of this model with the conductivity variation of the VAN films suggests that electron transport in $L_{1-x}Z_x$ composite films is mainly determined by a conducting network mechanism. In this composite system with a sufficient amount of conducting phase (LSMO), conducting channels are formed through coalescence of the LSMO nanodomains, as shown in previous TEM images. On the other hand, as the amount of LSMO decreases below a critical value (percolation threshold value 70% of ZnO molar ratio), the conducting channels will vanish and then the composite system exhibits tunneling or insulating behavior. The MIT temperature (T_{MIT}) of $L_{1-x}Z_x$ VAN films is plotted in the right axis, which also displays a systematic change from 284 to 150 K with the ZnO concentration when x increases from 0 to 50%. It is interesting to note that T_{MIT} of the $L_{0.5}Z_{0.5}$ film on buffered Si substrates (~150 K) is lower than that (~182 K) of the same VAN system on STO single-crystal substrates, which we demonstrated in a previous report.[14] Also, deposition of the $L_{0.5}Z_{0.5}$ film on buffered Si substrates also leads to a larger resistivity compared to that on STO substrates. The above performance is possibly due to domain matching of STO and TiN buffer layers on Si substrates increases phase boundaries and grain

boundaries in the upper VAN films, which suppressed the ferromagnetic (FM) double-exchange interaction between neighboring FM nanodomains.[27,28]

A more detailed study on LFMR of samples with different compositions has been conducted to explore the relationships of LFMR of the whole VAN system as a function of the ZnO phase x. Also, the resistivity ratio of $L_{1-x}Z_x$ composite films (x = 0, 0.3, 0.5, 0.7) was measured at 80 K with an external magnetic field from −1 to 1 T, as shown in Figure 4a. The

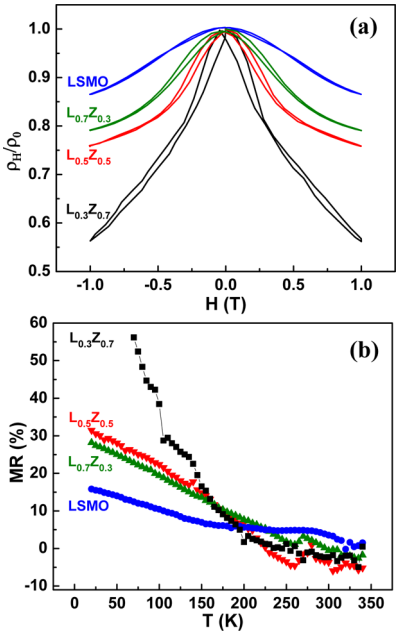

Figure 4. (a) Resistivity ratio ρ_H/ρ_0 composite films as a function of the magnetic field at 80 K. (b) MR as a function of the temperature with different compositions.

LFMR property of $L_{0.25}Z_{0.75}$ is not shown here, whose resistivity is beyond the measurement limit and becomes noisy in low temperature. It is interesting to note that all resistivity ratio curves show a sharp drop at a low field (0−0.5 T) for all compositions, followed by a more gradual drop at higher magnetic field (0.5−1 T). The one with the maximum MR is the composite film with 70% of ZnO molar ratio, which corresponds to the critical conduction threshold discussed above. The MR ratios of all samples are plotted in Figure 4b as a function of the temperature. The MR ratio here is defined by $MR = (\rho_0 - \rho_H)/\rho_0$, where ρ_0 is the zero-field resistivity and ρ_H is the resistivity under an applied magnetic field of 1 T. It is obvious that MR values of all samples increase gradually as the temperature decreases from room temperature to a low-temperature range. Also, the peak MR value for $L_{0.3}Z_{0.7}$ composite thin films on Si is 55%, which is comparable or superior to previous reports on thin films on Si substrates, such as polycrystalline LSMO thin films (MR = 16%; T = 77 K, and H = 0.3 T),[21] polycrystalline LSMO films (MR ≤ 20%; T = 77 K, and H = 0.4 T),[29] polycrystalline LSMO:Al_2O_3 composite films (MR = 15%; T = 86 K, and H = 0.3 T),[30] and bulk composites.[31,32] It is worth pointing out that the peak MR value (~32%) of the $L_{0.5}Z_{0.5}$ film on buffered Si substrates is close to that (~30%) deposited on STO single-crystal substrates,[14] which also implies the success of integration of the $L_{1-x}Z_x$ film on Si substrates. Also, the main difference between their LFMR performances is that the $L_{1-x}Z_x$ films on STO reached the peak MR value at a higher temperature, which relates to less spin-fluctuation depression due to decreased structural disorders, as discussed in the previous part. The enhanced and tunable LFMR of LSMO:ZnO composite thin films on Si substrates can be interpreted by spin-polarized tunneling based on magnetic tunnel junction structures. The large MR of LSMO:ZnO VAN films results from several aspects where a nonmagnetic insulating ZnO phase plays a significantly important role. First, the incorporation of ZnO creates artificial grain and phase boundaries where structural disorders contribute to the separation of neighboring FM domains, increase of the density of intergrain spin polarization, and promotion of spin-polarized tunneling. Second, the ZnO phase also serves as an insulating tunneling barrier, creating a "ferromagnetic-insulator" (FM-I) state and inducing local spin disorder.[33] It is suggested that epitaxial growth of LSMO:ZnO composite thin films on Si substrates contributes to the increase in the spin-polarized tunneling effect, resulting in better LFMR performance in the VAN films.

CONCLUSIONS

Highly epitaxial $(LSMO)_{1-x}:(ZnO)_x$ VAN thin films with various compositions were deposited on Si (001) substrates by PLD. STO and TiN bilayer buffer layers have been applied and proven to be an effective platform to grow epitaxial VAN films on Si. The tunable and enhanced LFMR property has been achieved by varying the ZnO concentration in the VAN films. The LFMR value reaches the maximum value of 55% with 70% of ZnO molar ratio at 70 K and 1 T. The incorporation of ZnO phases contributes to creating artificial grain and phase boundaries, increasing spin disorder and generating spin-polarized tunneling for the improved MR effect. Our results demonstrate that $(LSMO)_{1-x}:(ZnO)_x$ VAN architectures exhibit promising potential for future Si-based LFMR devices.

AUTHOR INFORMATION

Corresponding Author

*E-mail: wangh@ece.tamu.edu.

Notes

The authors declare no competing financial interest.

ACKNOWLEDGMENTS

The work was supported by the U.S. National Science Foundation (Ceramic Program, Grant NSF-1007969).

REFERENCES

(1) Ohtomo, A.; Hwang, H. Y. *Nature* **2004**, *427* (6973), 423−426.
(2) Salamon, M. B.; Jaime, M. *Rev. Mod. Phys.* **2001**, *73* (3), 583−628.
(3) Hambe, M.; Petraru, A.; Pertsev, N. A.; Munroe, P.; Nagarajan, V.; Kohlstedt, H. *Adv. Funct. Mater.* **2010**, *20* (15), 2436−2441.
(4) Yu, P.; Chu, Y.-H.; Ramesh, R. *Mater. Today* **2012**, *15* (7−8), 320−327.
(5) You, L.; Lu, C.; Yang, P.; Han, G.; Wu, T.; Luders, U.; Prellier, W.; Yao, K.; Chen, L.; Wang, J. *Adv. Mater.* **2010**, *22* (44), 4964−4968.
(6) Logvenov, G.; Gozar, A.; Bozovic, I. *Science* **2009**, *326* (5953), 699−702.
(7) Lebedev, O. I.; Verbeeck, J.; Van Tendeloo, G.; Shapoval, O.; Belenchuk, A.; Moshnyaga, V.; Damashcke, B.; Samwer, K. *Phys. Rev. B* **2002**, *66* (10), 104421.
(8) Zheng, H.; Straub, F.; Zhan, Q.; Yang, P. L.; Hsieh, W. K.; Zavaliche, F.; Chu, Y. H.; Dahmen, U.; Ramesh, R. *Adv. Mater.* **2006**, *18* (20), 2747−2752.

(9) MacManus-Driscoll, J. L.; Zerrer, P.; Wang, H. Y.; Yang, H.; Yoon, J.; Fouchet, A.; Yu, R.; Blamire, M. G.; Jia, Q. X. *Nat. Mater.* **2008**, *7* (4), 314−320.
(10) MacManus-Driscoll, J. L. *Adv. Funct. Mater.* **2010**, *20* (13), 2035−2045.
(11) Chen, A.; Bi, Z.; Jia, Q. X.; MacManus-Driscoll, J. L.; Wang, H. *Acta Mater.* **2013**, *61* (8), 2783−2792.
(12) Weal, E.; Patnaik, S.; Bi, Z.; Wang, H.; Fix, T.; Kursumovic, A.; Driscoll, J. L. M. *Appl. Phys. Lett.* **2010**, *97* (15), 153121−3.
(13) Bi, Z.; Lee, J. H.; Yang, H.; Jia, Q.; MacManus-Driscoll, J. L.; Wang, H. *J. Appl. Phys.* **2009**, *106* (9), 094309−5.
(14) Chen, A.; Bi, Z.; Tsai, C.-F.; Lee, J.; Su, Q.; Zhang, X.; Jia, Q.; MacManus-Driscoll, J. L.; Wang, H. *Adv. Funct. Mater.* **2011**, *21* (13), 2423−2429.
(15) Kang, B. S.; Wang, H.; MacManus-Driscoll, J. L.; Li, Y.; Jia, Q. X.; Mihut, I.; Betts, J. B. *Appl. Phys. Lett.* **2006**, *88* (19), 192514−192513.
(16) Chen, A. P.; Bi, Z. X.; Hazariwala, H.; Zhang, X. H.; Su, Q.; Chen, L.; Jia, Q. X.; MacManus-Driscoll, J. L.; Wang, H. Y., *Nanotechnology* **2011**, *22* (31), 315712.
(17) Levin, I.; Li, J.; Slutsker, J.; Roytburd, A. L. *Adv. Mater.* **2006**, *18* (15), 2044−2047.
(18) Schlom, D. G.; Chen, L.-Q.; Pan, X.; Schmehl, A.; Zurbuchen, M. A. *J. Am. Ceram. Soc.* **2008**, *91* (8), 2429−2454.
(19) Wang, H.; Foltyn, S. R.; Arendt, P. N.; Jia, Q. X.; Li, Y.; Zhang, X. *Phys. C* **2005**, *433* (1−2), 43−49.
(20) Wang, J.; Zheng, H.; Ma, Z.; Prasertchoung, S.; Wuttig, M.; Droopad, R.; Yu, J.; Eisenbeiser, K.; Ramesh, R. *Appl. Phys. Lett.* **2004**, *85* (13), 2574−2576.
(21) Goh, W. C.; Yao, K.; Ong, C. K. *J. Appl. Phys.* **2005**, *97* (7), 073905.
(22) Kim, J.-H.; Khartsev, S. I.; Grishin, A. M. *Appl. Phys. Lett.* **2003**, *82* (24), 4295−4297.
(23) Balcells, L.; Carrillo, A. E.; Martinez, B.; Fontcuberta, J. *Appl. Phys. Lett.* **1999**, *74* (26), 4014−4016.
(24) Gupta, S.; Ranjit, R.; Mitra, C.; Raychaudhuri, P.; Pinto, R. *Appl. Phys. Lett.* **2001**, *78* (3), 362−364.
(25) Toker, D.; Azulay, D.; Shimoni, N.; Balberg, I.; Millo, O. *Phys. Rev. B* **2003**, *68* (4), 041403.
(26) Dubson, M. A.; Garland, J. C. *Phys. Rev. B* **1985**, *32* (11), 7621−7623.
(27) Imada, M.; Fujimori, A.; Tokura, Y. *Rev. Mod. Phys.* **1998**, *70* (4), 1039−1263.
(28) Gupta, A.; Gong, G. Q.; Xiao, G.; Duncombe, P. R.; Lecoeur, P.; Trouilloud, P.; Wang, Y. Y.; Dravid, V. P.; Sun, J. Z. *Phys. Rev. B* **1996**, *54* (22), 15629−15632.
(29) Yang, S. Y.; Kuang, W. L.; Liou, Y.; Tse, W. S.; Lee, S. F.; Yao, Y. D. *J. Magn. Magn. Mater.* **2004**, *268* (3), 326−331.
(30) Yan, L.; Kong, L. B.; Yang, T.; Goh, W. C.; Tan, C. Y.; Ong, C. K.; Rahman, M. A.; Osipowicz, T.; Ren, M. Q. *J. Appl. Phys.* **2004**, *96* (3), 1568−1571.
(31) Valencia, S.; Castano, O.; Fontcuberta, J.; Martinez, B.; Balcells, L. *J. Appl. Phys.* **2003**, *94* (4), 2524−2528.
(32) Das, D.; Saha, A.; Russek, S. E.; Raj, R.; Bahadur, D. *J. Appl. Phys.* **2003**, *93* (10), 8301−8303.
(33) Gupta, A.; Sun, J. Z. *J. Magn. Magn. Mater.* **1999**, *200* (1−3), 24−43.